Semi-conducting mixed-valent $X_4TCNQ^{-I/-II}$ (X = H, F) charge-transfer complexes with $C_6H_2(NH_2)_4$

Ashley L. Sutton,[a] Brendan F. Abrahams,*[a] Deanna M. D'Alessandro,[b] Lars Goerigk,[a] Timothy A. Hudson,[a] Richard Robson,[a] Pavel M. Usov[b]

Electronic Supplementary Information

a. School of Chemistry, University of Melbourne, Victoria 3010, Australia
E-mail: bfa@unimelb.edu.au; Fax +61 3 9347 5180; Tel: +61 3 8344 0341
b. School of Chemistry, University of Sydney, New South Wales, 2006, Australia.

S1 Synthesis

$[C_6H_2(NH_2)_4][TCNQ]$

$[C_6H_2(NH_2)_4][TCNQ]$ was prepared according to the literature procedure.[1] IR (KBr) ν: 2179, 2144 cm^{-1}.

$[C_6H_2(NH_2)_4][F_4TCNQ]$

A solution of F_4TCNQH_2 (13.9 mg, 0.05 mmol) in methanol (1.5 mL) and N,N-dimethylformamide (0.5 mL) was added to a stirred suspension of $[C_6H_2(NH_2)_2(NH)_2]$ (6.5 mg, 0.05 mmol) in methanol (1.0 mL). The reaction mixture was stirred for several hours during which time a dark precipitate formed. The solid was collected by filtration and washed with methanol (7.2 mg, 35 %). IR (KBr) ν: 2181, 2149 cm^{-1}.

Infrared spectra were collected on a Bruker Tensor 27 FT-IR using pressed KBr discs.

S2 Powder diffraction

Powder x-ray diffraction patterns were collected on either an Oxford Diffraction SuperNova or a XtaLAB Synergy diffractometer. Data were collected on the lab-based instruments using Cu Kα radiation. Data collected were processed with the CrysAlisPro software and a baseline correction performed. Sample temperature was held using a stream of N_2 gas controlled by a Cryostream device.

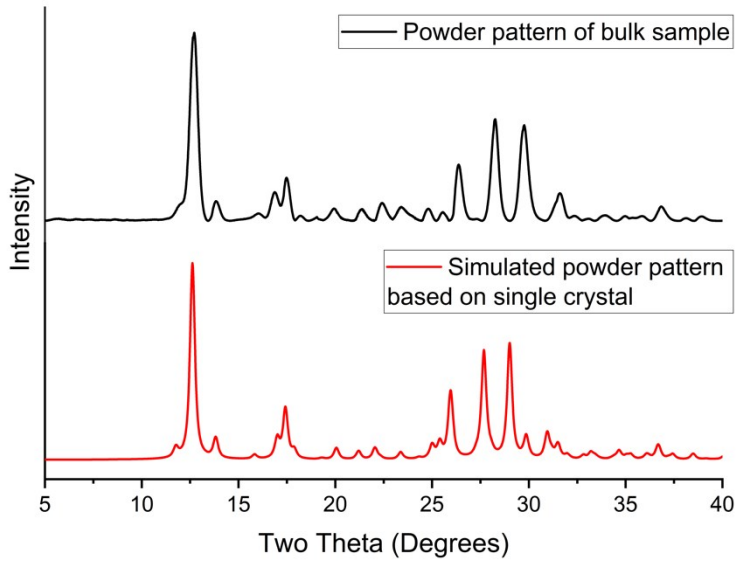

Fig. S2.1 Powder diffraction pattern of $[C_6H_2(NH_2)_4][TCNQ]$.

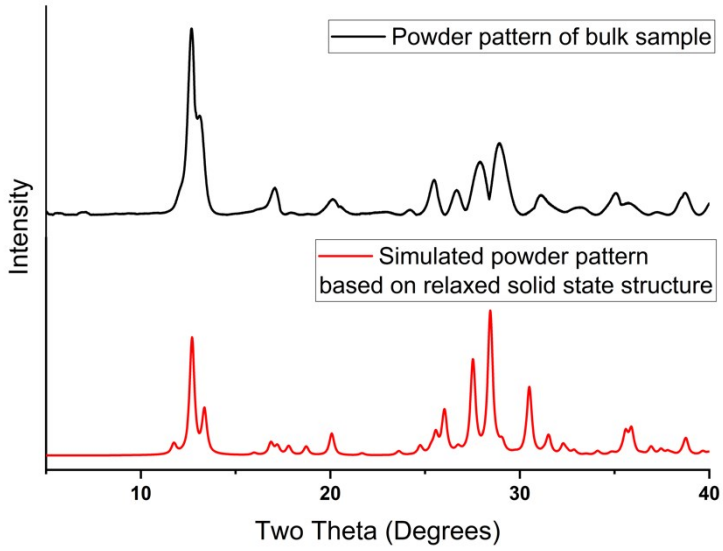

Fig. S2.2 Powder diffraction pattern of $[C_6H_2(NH_2)_4][F_4TCNQ]$.

S3 Kistenmacher relationship calculations

The Kistenmacher relationship can be used to relate selected bond distances within the X_4TCNQ unit to estimate the charge associated with the X_4TCNQ species.[2]

The relationship is given by the expression:

$$q = -A[c/(b + d)] + B$$

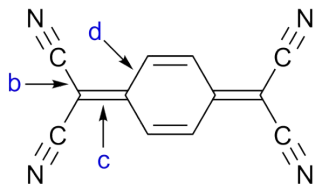

Recent work with the dianionic forms of X_4TCNQ has enabled the calculation of revised values for A and B for both TCNQ (A = -41.667, B = 19.818) and F_4TCNQ (A = -45.756, B = 21.846).[3] These values have been used to estimate the charge associated with the X_4TCNQ in the charge-transfer complexes reported.

Table S3.1 Selected bond lengths within the X_4TCNQ species of the $[C_6H_2(NH_2)_4][X_4TCNQ]$ complexes.

CT complex	***b* (Å)**	***c* (Å)**	***d* (Å)**	***c*/(*b*+*d*)**	**Charge (*q*)**
$[C_6H_2(NH_2)_4][TCNQ]$	1.409(4)	1.435(3)	1.411(4)	0.509	-1.39(12)
$[C_6H_2(NH_2)_4][F_4TCNQ]$[a]	1.401	1.443	1.412	0.513	-1.63

[a] Bond lengths are from the relaxed dispersion-corrected DFT structure.

S4 Infra-red spectroscopic analysis of charge transfer

The general empirical formula:

$$\rho = 2\Delta\nu/\nu_0(1 - \nu_1^2/\nu_0^2)^{-1}$$
$$\textit{where } \Delta\nu = \nu_0 - \nu_{CT}$$

has been widely used for both TCNQ[4, 5] and F_4TCNQ[6, 7] based charge-transfer complexes and relates the infrared frequencies of the localised (ν_0, ν_1) and charge-transfer (ν_{CT}) species to the degree of charge-transfer (ρ). The method has been applied to X_4TCNQ based CT systems in which the X_4TCNQ acts as an acceptor, however in this current work the X_4TCNQ species is a donor. As such ν_0 is assigned as the localised dianionic state and ν_1 as the localised radical anionic state.

Typically, for neutral TCNQ the ν(CN) stretches occur at 2225 while for the radical monoanion the ν(CN) stretches are lowered to 2187 and 2158 cm^{-1}. Further reduction to 2152 and 2104 cm^{-1} occurs for the dianion.[1, 8] The nitrile frequencies of $[C_6H_2(NH_2)_4]$[TCNQ] are 2179 and 2144 cm^{-1}. With frequencies of 2152 cm^{-1}, 2187 cm^{-1} and 2179 cm^{-1} for ν_0, ν_1 and ν_{CT} respectively, ρ = 0.77 corresponding to a charge of -1.23. In contrast the electron withdrawing fluorine substituents of F_4TCNQ, result in nitrile shifts to higher energies, typically at 2225 cm^{-1} for the neutral system, 2197 and 2178 cm^{-1} for the radical monoanion and at 2167 and 2133 cm^{-1} for the dianion.[9, 10, 11, 12] The nitrile frequencies of $[C_6H_2(NH_2)_4]$[F_4TCNQ] are 2181 and 2149 cm^{-1}. With frequencies of 2167 cm^{-1}, 2197 cm^{-1} and 2181 cm^{-1} for ν_0, ν_1 and ν_{CT} respectively, ρ = 0.46 corresponding to a charge of -1.54.

S5 Degree of charge transfer (*p*) and charge (*q*) of X_4TCNQ

The X_4TCNQ species can act as both an electron donor and an electron acceptor. The charge (*q*) on the X_4TCNQ species can be used to infer the degree of charge transfer (*p*) within the CT complex. Figure S4.1 highlights this case for TCNQ species.

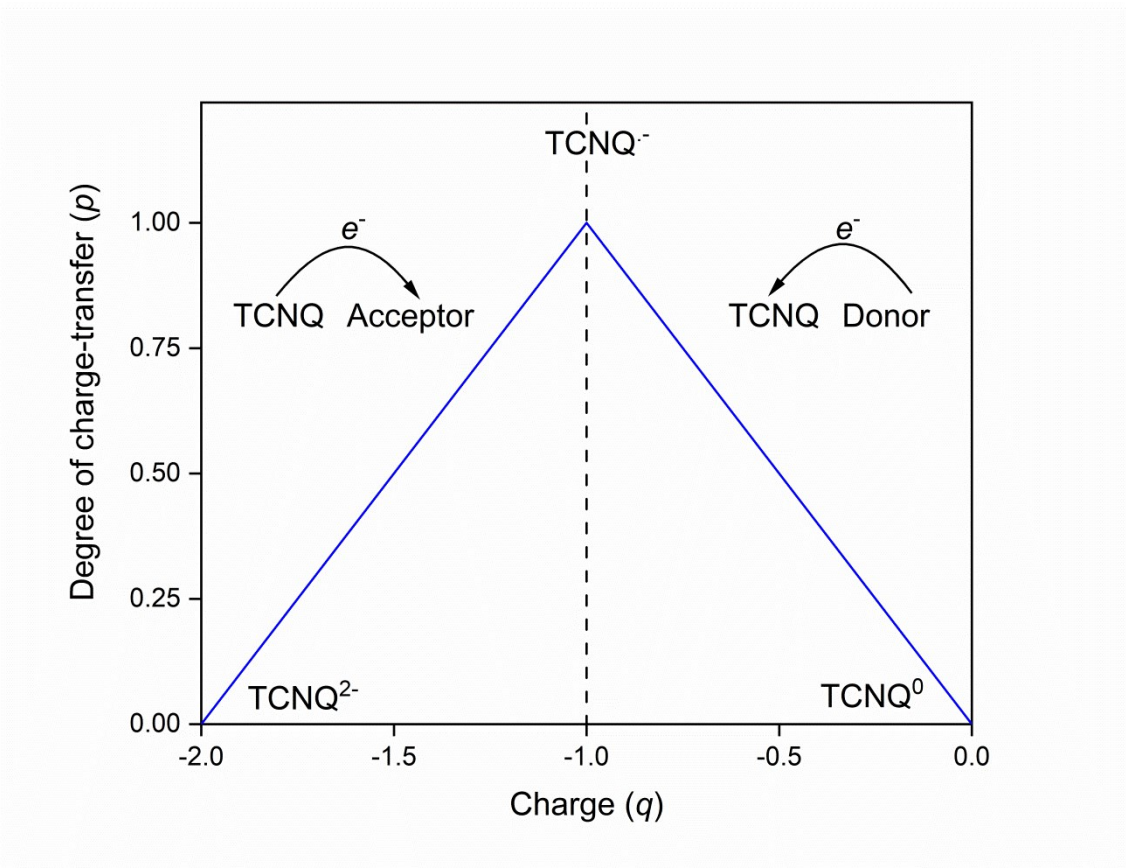

Fig. S5.1 Degree of charge transfer (*p*) from donor to acceptor represented schematically as function of the charge on the TCNQ species.

S6 UV-Vis-NIR spectroscopy

Vis-NIR diffuse reflectance spectroscopy was used to analyse powdered samples. The spectrum was collected on a CARY 5000 UV-Vis-NIR spectrophotometer with a Harrick Omni Diff Probe attachment using Varian WinUV software V3.0. The data were recorded from 5000 to 25 000 cm^{-1} with a scan rate of 6000 cm^{-1} min^{-1}. Samples were supported on high density filter paper which was also used to provide the background reference. The Kubelka–Munk transform has been applied to produce a Tauc plot where $F(R) = (1 - R)^2/2R$ (R is the diffuse reflectance of the sample as compared to the background reference).

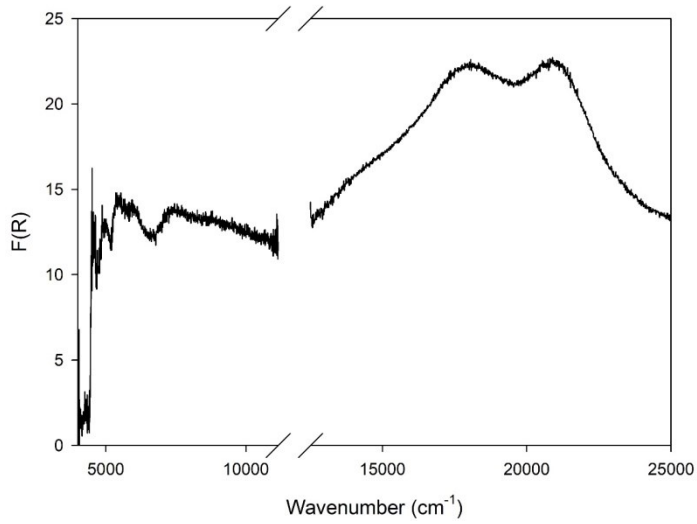

Fig. S6.1 Vis-NIR spectra of $[C_6H_2(NH_2)_4][TCNQ]$. The axis break corresponds to the discontinuity at the detector changeover.

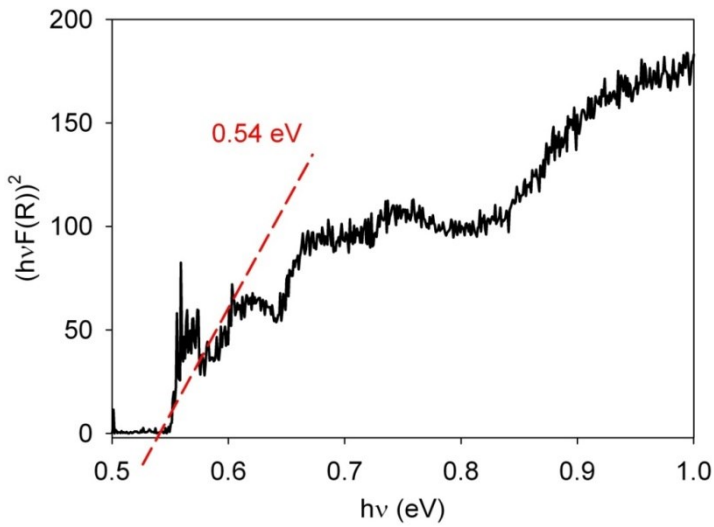

Fig. S6.2 Tauc plot for $[C_6H_2(NH_2)_4][TCNQ]$ CT complex showing the bandgap.

S7 Electrical conductivity measurements

Two point conductivity measurements were conducted with an in-house constructed apparatus, with a 2-electrode screw cell design adapted from reference [13]. Pellets of the compound were pressed between two copper dies (contact area 7.069 mm^2) with two brass screws (see Figure S6.1). Sample thickness was measured with callipers and was in the range of 0.1 mm. The assembled screw cell was placed in an in-house built cryostat to achieve temperature control. I-V profiles were recorded with an Ossila X100 Source Measure Unit.

The conductivity of the material was calculated from the I-V profiles by modelling with Ohm's law, $R = \frac{V}{I}$, where R is resistance, V is voltage and I is current

The temperature dependence of the conductivity was fitted to the Arrhenius equation, $\sigma = \sigma_o e^{\frac{-Ea}{k_B T}}$, where σ is the conductivity, σ_o is the pre-exponential factor, Ea is the activation energy, k_B is the Boltzmann constant and T is the temperature.

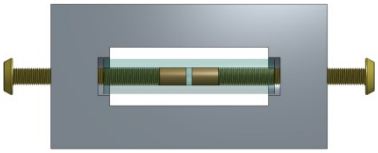

Fig. S7.1 Two point screw-cell design used for electrical conductivity measurements.

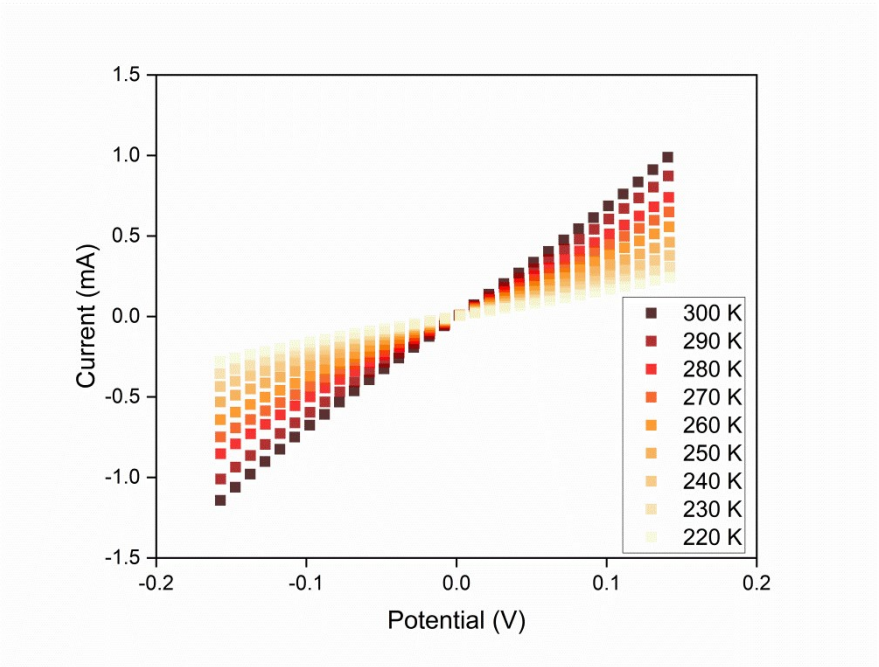

Fig. S7.2 I-V curves for the $[C_6H_2(NH_2)_4][TCNQ]$ compound.

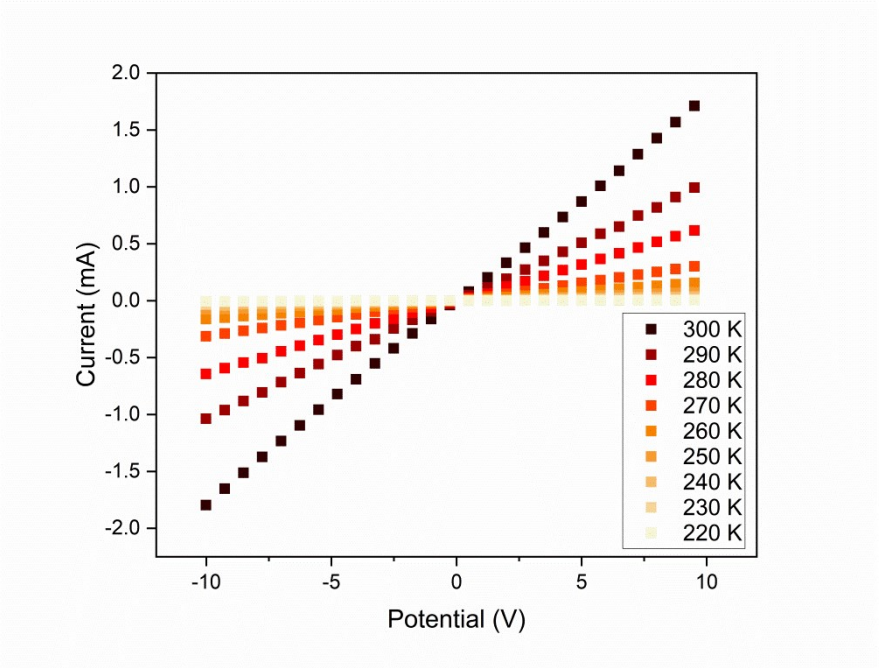

Fig. S7.3 I-V curves for the $[C_6H_2(NH_2)_4][F_4TCNQ]$ compound.

S8 Computational details, band structure and density of states (DOS) plots

Electronic-structure calculations have been undertaken with the projected augmented wave (PAW) formalism combined with plane-wave based, periodic Density Functional Theory (DFT), as implemented within the Vienna Ab-initio Simulation Package (VASP). [14-16]

The single crystal structure of the $[C_6H_2(NH_2)_4]$[TCNQ] complex was known.[1] An input file was prepared from crystallographic data with the aid of the Bilbao Crystallographic Server resources. The atomic positions of the $[C_6H_2(NH_2)_4]$[TCNQ] structure were allowed to relax with fixed lattice constants using the Perdew-Burke-Ernzerhof functional (PBE).[17] As van der Waals effects are expected to influence the structure, Grimme's DFT-D3 dispersion correction with Becke-Johnson damping in its periodic implementation has been applied.[18] The validity of the relaxed structure was supported by comparison of the TCNQ bond lengths to the single crystal structure (Table S8.1). With these values within the expected tolerances for a generalised gradient approximation (GGA) functional,[19] such as PBE(-D3). After preliminary tests – as is common for such cases – a plane-wave cutoff energy of 500 eV was found suitable for convergence of the electronic wave functions to give total energies within an accuracy of 0.01 eV/atom and was used for all calculations. A gamma centered *k*-mesh (5 x 4 x 3) was employed for the structure optimisation.

Crystallographic atomic positional data could not be obtained for $[C_6H_2(NH_2)_4][F_4TCNQ]$. Powder x-ray diffraction indicates however that the structure of $[C_6H_2(NH_2)_4][F_4TCNQ]$ is similar to $[C_6H_2(NH_2)_4]$[TCNQ]. The crystallographic positions from the $[C_6H_2(NH_2)_4]$[TCNQ] structure were used as initial inputs, with the hydrogen atoms of the TCNQ species replaced with fluorone atoms. The lattice parameters and atomic positions were relaxed with the PBE-D3(BJ) level of theory and a plane wave cutoff energy of 1000 eV - which was sufficient to relieve Pulay stress.[20] The powder pattern of the $[C_6H_2(NH_2)_4][F_4TCNQ]$ relaxed structure compares favourably with the experimental powder pattern for this compound.

Key electronic properties (band structures and density of states) were calculated with single-point calculations with the HSE06[21] functional based on the PBE-D3(BJ) optimised structures. Electronic band-structures were calculated along high symmetry points according to the Bilbao Crystallographic Server.[22-24] The density of states were calculated with a gamma centered *k*-

mesh (5 x 4 x 3). The separation into partial density of states (PDOS) was carried out with a group-own code.

Band decomposed charge density plots were generated in Visualization for Electronic and STructural Analysis (VESTA, available from http://jp-minerals.org/vesta/en/).

Table S8.1 Bond distances of the TCNQ within the $[C_6H_2(NH_2)_4][TCNQ]$ complex as determined by single-crystal X-ray diffraction and solid-state DFT.

	a (Å)	**b (Å)**	**c (Å)**	**d (Å)**	**e (Å)**
Single crystal	1.147(4)	1.409(4)	1.435(3)	1.402(4)	1.366(3)
DFT	1.177	1.398	1.452	1.416	1.384
Difference (Å)	+0.030	-0.011	+0.017	+0.014	+0.018
	+2.6%	-0.78%	+1.2%	+1.0%	+1.3%

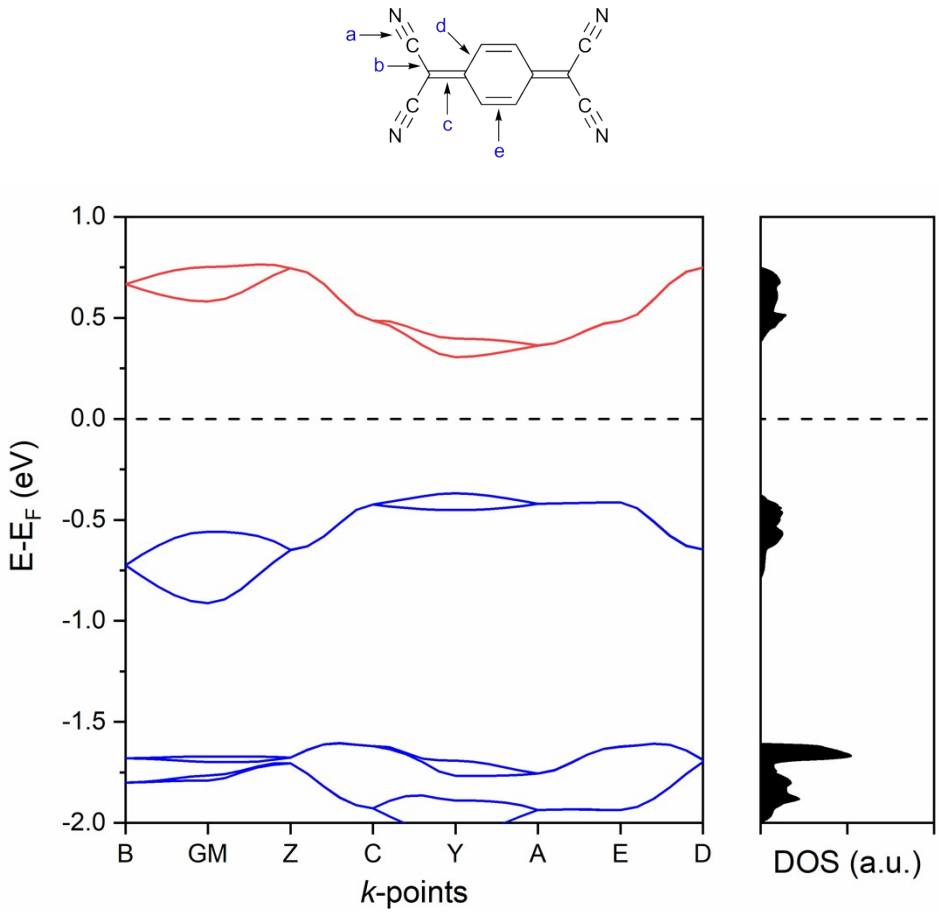

Fig. S8.1 Band structure and DOS for $[C_6H_2(NH_2)_4][F_4TCNQ]$.

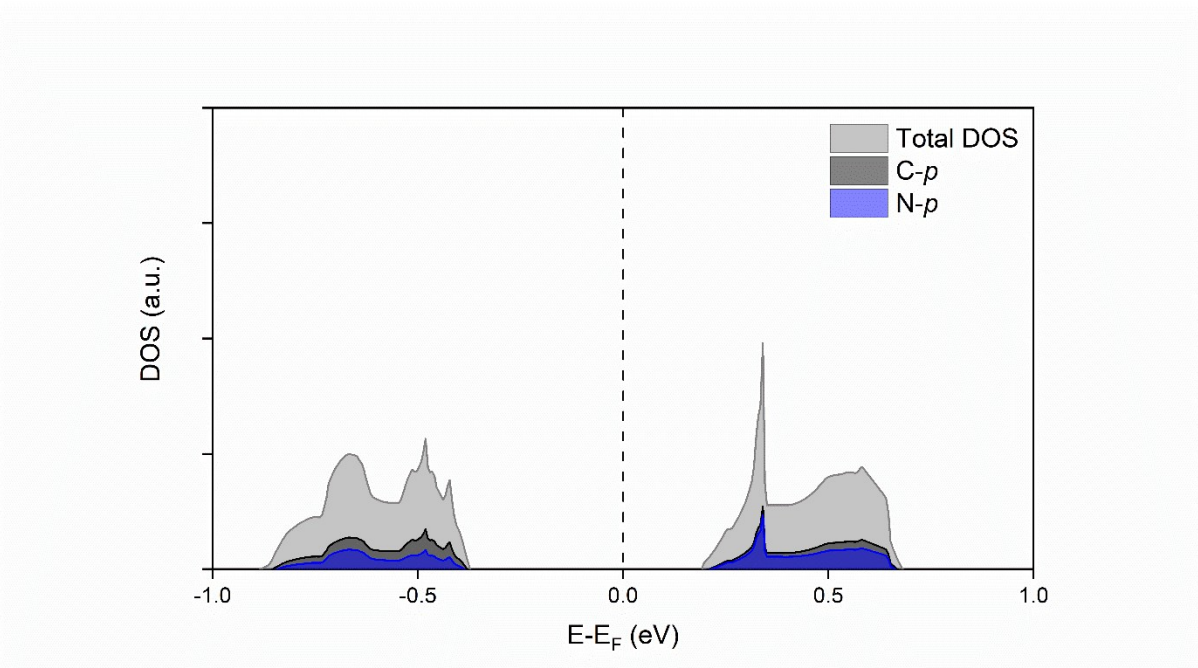

Fig. S8.2 Partial density of states plot for $[C_6H_2(NH_2)_4][TCNQ]$.

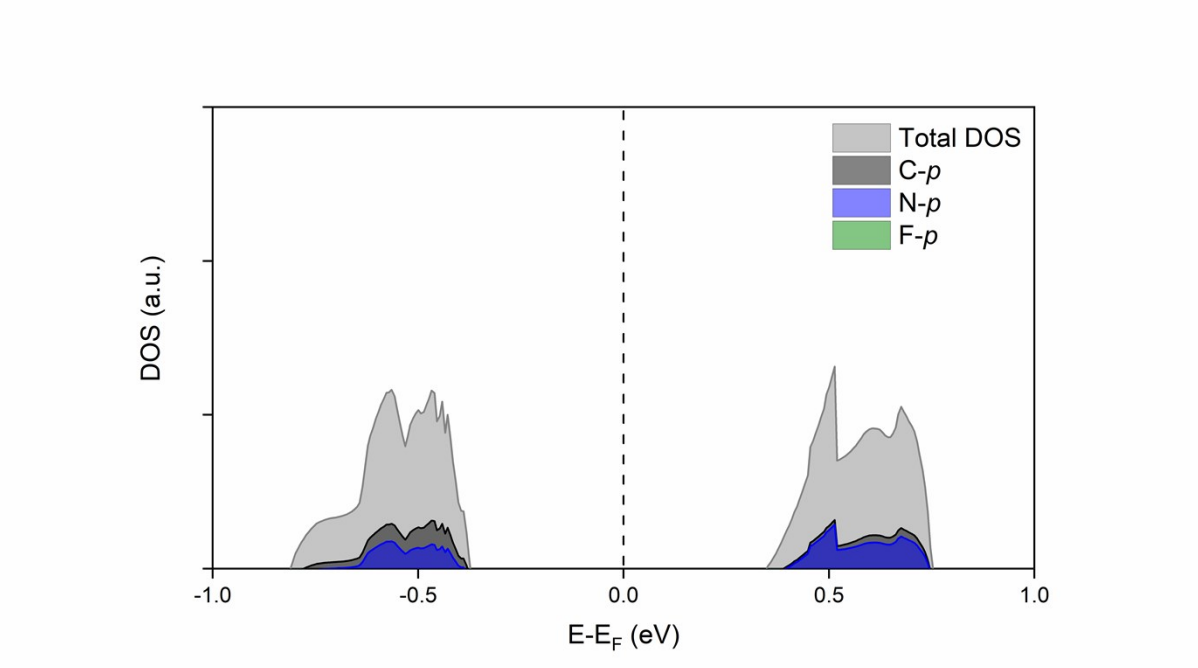

Fig. S8.3 Partial density of states plot for $[C_6H_2(NH_2)_4][F_4TCNQ]$.

Table S8.2 Band gaps and band dispersions for $[C_6H_2(NH_2)_4][TCNQ]$ and $[C_6H_2(NH_2)_4][F_4TCNQ]$.

CT complex	**Band gap (eV)**	**Valence bandwidth (eV)**	**Conduction bandwidth (eV)**
$[C_6H_2(NH_2)_4][TCNQ]$	0.49	0.45	0.50
$[C_6H_2(NH_2)_4][F_4TCNQ]$	0.67	0.36	0.44

S9 References

1. T. A. Hudson and R. Robson, *Cryst. Growth Des.*, 2009, **9**, 1658-1662.
2. T. J. Kistenmacher, T. J. Emge, A. N. Bloch and D. O. Cowan, *Acta Crystallogr. B*, 1982, **38**, 1193-1199.
3. A. L. Sutton, B. F. Abrahams, D. M. D'Alessandro, R. W. Elliott, T. A. Hudson, R. Robson and P. M. Usov, *CrystEngComm*, 2014, **16**, 5234-5243.
4. T. J. Kistenmacher, T. J. Emge, F. M. Wiygul, W. A. Bryden, J. S. Chappell, J. P. Stokes, L. Y. Chiang, D. O. Cowan and A. N. Bloch, *Solid State Commun.*, 1981, **39**, 415-417.
5. E. Kampar and O. Neilands, *Russ. Chem. Rev.*, 1986, **55**, 334-342.
6. P. Hu, H. Li, Y. Li, H. Jiang and C. Kloc, *CrystEngComm*, 2017, **19**, 618-624.
7. P. Hu, K. Du, F. Wei, H. Jiang and C. Kloc, *Cryst. Growth Des.*, 2016, **16**, 3019-3027.
8. T. Takenaka, *Bulletin of the Institute for Chemical Research*, 1969, **47**, 387-400.
9. T. H. Le, A. P. O'Mullane, L. L. Martin and A. M. Bond, *J Solid State Electrochem*, 2011, **15**, 2293-2304.
10. C. Ouyang, Y. Guo, H. Liu, Y. Zhao, G. Li, Y. Li, Y. Song and Y. Li, *J. Phys. Chem. C*, 2009, **113**, 7044-7051.
11. S. A. O'Kane, R. Clérac, H. Zhao, X. Ouyang, J. R. Galán-Mascarós, R. Heintz and K. R. Dunbar, *J. Solid State Chem.*, 2000, **152**, 159-173.
12. D. A. Dixon, J. C. Calabrese and J. S. Miller, *J. Phys. Chem.*, 1989, **93**, 2284-2291.
13. L. E. Darago, M. L. Aubrey, C. J. Yu, M. I. Gonzalez and J. R. Long, *J. Am. Chem. Soc.*, 2015, **137**, 15703-15711.
14. G. Kresse and J. Hafner, *Phys. Rev. B*, 1994, **49**, 14251-14269.
15. G. Kresse and J. Furthmüller, *Comput. Mater. Sci.*, 1996, **6**, 15-50.
16. G. Kresse and J. Furthmuller, *Phys. Rev. B*, 1996, **54**, 11169-11186.
17. J. P. Perdew, K. Burke and M. Ernzerhof, *Phys. Rev. Lett.*, 1996, **77**, 3865-3868.
18. S. Grimme, S. Ehrlich and L. Goerigk, *J. Comput. Chem.*, 2011, **32**, 1456-1465.
19. K. E. Riley, B. T. Op't Holt and K. M. Merz, Jr., *J. Chem. Theory Comput.*, 2007, **3**, 407-433.
20. G. P. Francis and M. C. Payne, *J. Phys. Condens. Matter*, 1990, **2**, 4395-4404.
21. A. V. Krukau, O. A. Vydrov, A. F. Izmaylov and G. E. Scuseria, *J. Chem. Phys.*, 2006, **125**, 224106.
22. M. I. Aroyo, J. M. Perez-Mato, D. Orobengoa, E. Tasci, G. de la Flor and A. Kirov, *Bulg. Chem. Commun.*, 2011, **43**, 183-197.
23. M. I. Aroyo, J. M. Perez-Mato, C. Capillas, E. Kroumova, S. Ivantchev, G. Madariaga, A. Kirov and H. Wondratschek, *Z. Kristallogr. Cryst. Mater.*, 2006, **221**, 15–27.
24. M. I. Aroyo, A. Kirov, C. Capillas, J. M. Perez-Mato and H. Wondratschek, *Acta Crystallogr. A*, 2006, **62**, 115-128.